Andean Geology 50 (2): 181-200. May, 2023 doi: 10.5027/andgeoV50n2-3503

Compositional and geothermobarometric analysis of the Upper Miocene tholeiitic volcanic products in the northern Andes at 5-6° N latitude: The Combia Volcanic Province

*Natalia Villalba¹, Hugo Murcia².³,⁴, Edith Jerez⁵, Daniel Piedrahita⁴, Dayana Schonwalder-Ángel⁵, Andrés Pardo-Trujillo².³,⁴, Sebastián Echeverri³,⁴

¹ Maestría en Ciencias de la Tierra, Universidad Nacional Autónoma de México, Cto. de los Posgrados S/N, C.U., Coyoacán, CP 04510, Ciudad de México, CDMX.

natalia.villalba@gmail.com

- ² Departamento de Ciencias Geológicas, Universidad de Caldas, Cl. 65 #26-10, Manizales, CP 170004, Caldas, Colombia. hugo.murcia@ucaldas.edu.co; andres.pardo@ucaldas.edu.co
- ³ Instituto de Investigaciones en Estratigrafía (IIES), Universidad de Caldas, Cl. 65 #26-10, Manizales, CP 170004, Caldas, Colombia. sebastian.echeverri@ucaldas.edu.co
- ⁴ Grupo de Investigación en Estratigrafía y Vulcanología (GIEV) "Cumanday", Cl. 65 #26-10, Manizales, CP 170004, Caldas, Colombia. danielpt 93@hotmail.com
- ⁵ Escuela de Geología, Universidad Industrial de Santander, Cra. 27 #9 Ciudad Universitaria, CP 680002, Bucaramanga, Santander, Colombia.

calimakt@hotmail.com; dschonwa@uis.edu.co

ABSTRACT. The Combia Volcanic Province (~11-5 Ma), is a volcaniclastic sequence located in northwest Colombia between the Central and Western cordilleras at 5-6° N latitude. Its source is associated with the volcanic activity of the magmatic arc produced by the subduction of the Nazca plate under the South American plate in the northern Andes. The distribution, composition, and chronostratigraphy of the province's deposits are well-known, with the volcanic sequences characterized as compositionally bimodal. The older rocks (ca. 11-9 Ma) display tholeitic affinity, whereas the younger (ca. 9-5 Ma) are mostly calc-alkaline, with some adakite-like signature recognized. While the magmatic system for the calc-alkaline magmas has been previously extensively studied, the processes that occurred during the magma stagnation and ascent are unknown for the tholeittic magmas. This work bridges this gap by the study of tholeiitic lava flows outcropping at the center of the province, through petrography, mineral chemistry, whole-rock analysis, and geothermobarometry calculations of the crystallization conditions. Texturally, the rocks are porphyritic with plagioclase (An_{50.90}) and clinopyroxene (augite and pigeonite) phenocrysts and microphenocrysts, embedded in a glassy and microcrystalline groundmass. Compositionally, the rocks vary from basaltic andesite to andesite (52.8-57.8 wt% SiO₂), with relative enrichments of LILE to HFSE and REE to chondrite. Crystallization conditions, based on several plagioclase-melt and pyroxene-melt geothermobarometers, were estimated at T=1,095-1,153 °C and P=0.22-0.60 GPa for the plagioclase, T=1,046-1,131 °C and P=0.09-0.21 GPa for the augite, and T=867-1,039 °C and P=0.40-0.60 GPa for the pigeonite. These results suggest a relatively rapid magma ascent for the tholeitic products as well as an evolution mostly through fractional crystallization. The LILE elements enrichment, the negative trend in the FeOt, TiO, and CaO versus SiO, content, together with some disequilibrium textures, are also evidence of crustal contamination and magma recharge. Thus it is proposed that the Combia Volcanic Province started as a simple magmatic system, where the tholeiitic products were generated by a relatively rapid magma ascent. Then, a more complex magmatic system linked to long-term magma stagnation, allowed melt evolution to form calc-alkaline magmas as previously defined.

Keywords: Andean Miocene volcanism, Tholeitic magmas, Geothermobarometry.

^{*}Corresponding author: nataliai.villalbam@gmail.com

RESUMEN. Análisis composicional y geotermobarométrico de los productos volcánicos toleíticos del Mioceno Superior en el norte de los Andes (latitud 5-6°): Provincia Volcánica Combia. La Provincia Volcánica Combia (~11-5 Ma) es una secuencia volcanoclástica ubicada al noroeste de Colombia, entre las cordilleras Central y Occidental en las latitudes 5-6° N. Su fuente se asocia a la actividad volcánica del arco producido por la subducción de la placa Nazca bajo la placa Sudamericana en la parte norte de los Andes. La distribución, composición y cronoestratigrafía de los depósitos de esta provincia se encuentran bien definidos, siendo las secuencias volcánicas caracterizadas composicionalmente como bimodales. Las rocas más antiguas (ca. 11-9 Ma) son de afinidad toleítica y las más jóvenes (ca. 9-5 Ma) son mayormente calcoalcalinas, con firmas adakíticas. A pesar de que el sistema magmático de formación de los magmas toleíticos ha sido ampliamente estudiado, los procesos ocurridos durante el estancamiento y ascenso del magma toleítico aún son desconocidos. Este trabajo presenta información nueva sobre estos productos que afloran como flujos de lava en el centro de la provincia, a través de análisis de petrografía, química mineral y de roca total, y cálculos de geotermobarometría para determinar las condiciones de cristalización. Texturalmente, las rocas son porfiríticas con fenocristales y microfenocristales de plagioclasa (An₅₀₋₉₀) y clinopiroxeno (augita y pigeonita) en una masa fundamental vítrea y microcristalina. Composicionalmente, las rocas varían entre andesita basáltica y andesita (52,8-57,8 wt % SiO₂), con enriquecimientos relativos de LILE en relación con HFSE y REE a condrito. Las condiciones de cristalización, con base en geotermobarómetros de plagioclasa-fundido y piroxeno-fundido, se estimaron en T=1.095-1.153 °C y P=0,22-0,60 GPa para la plagioclasa, T=1.046-1.131 °C y P=0,09-0,21 GPa para la augita, y T=867-1.039 °C y P=0,40-0,60 GPa para la pigeonita. Los resultados sugieren un ascenso relativamente rápido para los productos toleíticos, así como una evolución principalmente por cristalización fraccionada. El enriquecimiento en elementos LILE, las tendencias negativas en los contenidos de FeOt, TiO, y CaO versus SiO,, al igual que algunas texturas de desequilibrio, son evidencia de contaminación cortical y episodios de recarga de magma. Así, se propone que la Provincia Volcánica Combia comenzó como un sistema magmático simple, donde los productos toleíticos se generaron por un ascenso de magma relativamente rápido. Luego, un sistema magmático más complejo, ligado a estancamiento de magma a largo plazo, permitió la evolución del fundido para formar magmas calcoalcalinos, como se ha definido previamente.

Palabras clave: Vulcanismo mioceno de los Andes, Magmas toleíticos, Geotermobarometría.

1. Introduction

The Combia Volcanic Province (CVP) commonly known as Combia Formation (Grosse, 1926; Jaramillo, 1976; Duque-Caro, 1990; Sierra et al., 2005) is an Upper Miocene volcaniclastic sequence (~11-5 Ma; Restrepo et al., 1981; Tassinari et al., 2008; Jaramillo et al., 2019; Weber et al., 2020; Santacruz et al., 2021) consisting of lava flows, primary volcaniclastic deposits (fall and pyroclastic density currents) and secondary deposits (debris avalanches and lahars; Piedrahita et al., 2019), as well as subvolcanic bodies (Marriner and Millward, 1984; Ramírez et al., 2006; Tejada et al., 2007; Borrero and Toro-Toro, 2016; Bissig et al., 2017; Jaramillo et al., 2019; Santacruz et al., 2021). This volcanic province, which covers an area of ~1,300 km², is distributed in the Middle Cauca Belt (MCB), in the Amagá basin, between the Central and Western cordilleras in the Colombian Andes at 5-6° N latitude (López et al., 2006; Sierra and Marín-Cerón, 2011; Fig. 1A). It is considered as one of the first volcanic expression from the post-collisional magmatic arc generated by the re-established Nazca plate subduction under the South American plate

after the Panamá arc-continent collision (Wagner et al., 2017; Jaramillo et al., 2019; Weber et al., 2020).

The CVP exhibits a bimodal composition of tholeiitic (ca. 11-9 Ma) and calc-alkaline rocks, some of the latter with adakite-like signature (ca. 9-5 Ma; Borrero and Toro-Toro, 2016; Jaramillo et al., 2019; Bernet et al., 2020; Weber et al., 2020). All products host plagioclase as a ubiquitous mineral, although they also host olivine, pyroxene, amphibole, biotite and/or garnet in different proportions (Jaramillo et al., 2019; Weber et al., 2020). Recent studies have recognized that the lava flows and only some volcaniclastic products of basaltic and basaltic andesitic composition are the tholeiites, while most of the volcaniclastic products and all subvolcanic bodies of andesitic and dacitic composition display calc-alkaline signature (Jaramillo et al., 2019; Weber et al., 2020; Santacruz et al., 2021). To explain this bimodal chemical signature, several geological scenarios have been proposed based on different compositional analyzes, which can be simplified as follow: 1) Local thinning in the crust that allowed diverse evolution of the tholeiitic magmas; this based on trace elements ratios (Sr/Y, La/Yb, and Ce/Y; Jaramillo et al., 2019); 2) Various magma origins that

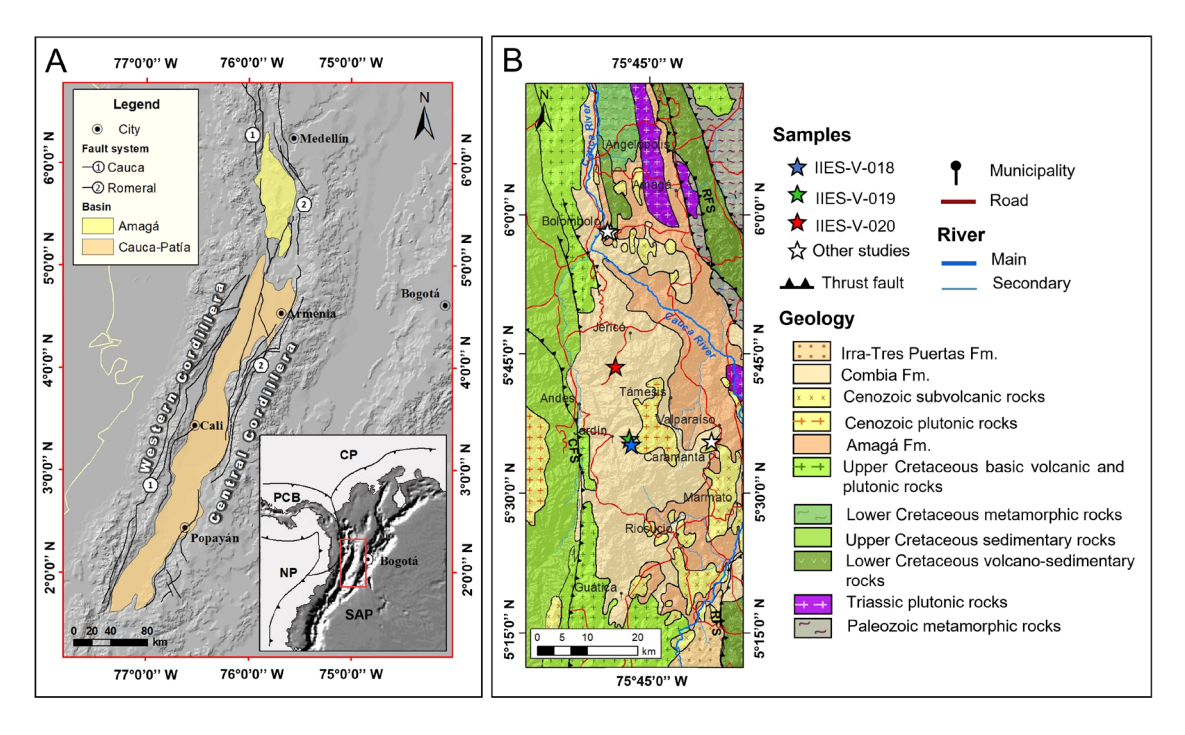


FIG. 1. A. Geographic location of the Amagá/Cauca-Patía basins; modified from Sierra and Marín-Cerón (2011). CP: Caribbean Plate, NP: Nazca Plate, PCB: Panamá-Chocó Block, SAP: South American Plate. B. Geologic map of the Amagá basin; modified from Sierra and Marín-Cerón (2011), RFS: Romeral Fault System, CFS: Cauca Fault System. White stars correspond to lava flows studied by Borrero and Toro-Toro (2016) and Jaramillo et al. (2019).

mixed during ascent plus the involvement of sediments and fluids from the subducting plate; this based on isotopic ratios (Nd, Pb, Sr; Bernet *et al.*, 2020); and **3)** Magma stagnation zones and mixing processes that allowed differential evolution and therefore different compositions; this based on trace elements ratios (*e.g.*, La/Yb and La/Sm), mineral chemistry (garnet and amphibole), and geothermobarometry analyses (Bernet *et al.*, 2020; Weber *et al.*, 2020).

Despite the above, there is still a great interest in understanding the configuration of the magmatic feeding system in order to document the characteristics of the magmatic arc associated with the re-established subduction of the Nazca plate during the Late Miocene after the arc-continent collision of the Panamá block. This paper provides lacking information about the magmatic evolution and crystallization conditions for the initial tholeiitic magma that gave origin to the CVP, based on petrographic characterizations, mineral and whole-rock chemical analyses and the geothermobarometric estimates for the crystallization conditions of the main mineral phases recognized. This approach, integrated with existing information, constitutes a contribution to understand the evolution

of the Andean magmatic arcs in post-collisional tectonic scenarios.

2. Geological Setting

The northwestern margin of South America has been subjected to collision of oceanic Plateaus and island arcs alternated with subduction episodes from the Late Cretaceous to Present-day associated with the interactions between the South American, Caribbean, Farallon/Nazca plates, and the Panamá-Chocó arc (e.g., Villagómez and Spikings, 2013; León et al., 2018; Montes et al., 2019; Zapata et al., 2020). These episodes seemingly provided first-order controls on the Cenozoic tectono-magmatic evolution of the continental arc in the Colombian Andes (e.g., Bayona et al., 2012; Echeverri et al., 2015; Wagner et al., 2017; Jaramillo et al., 2019). Towards the west of the Colombian Andes at 2-6° N latitude the history of this tectonic scenario and the tectono-magmatic evolution is recorded in hinterland basins controlled by strike-slip structures from the Eocene to Present-day, such as Amagá and Cauca/Patía basins (e.g., Sierra et al., 2005; Jaramillo et al., 2019; Bernet

2020; Weber et al., 2020; Gallego-Ríos et al., 2020). These basins are located between the Central and Western cordilleras with structural boundaries defined by the Romeral Fault System (RFS) to the east and Cauca Fault System (CFS) to the west (Fig. 1A). The eastern limb of the Amagá basin, which is the object of this study, exposes an assemblage of Paleozoic, Triassic, and Cretaceous metamorphic, plutonic and volcano-sedimentary rocks from Central Cordillera basements (Fig. 1B). The western limb exposes mafic volcanic and plutonic rocks with sedimentary pelagic rocks interlayering related to Caribbean allochthonous terrains accreted during the Late Cretaceous to the South American margin (Fig. 1B; Villagómez and Spiking, 2013; Spikings et al., 2015; Zapata et al., 2020).

The stratigraphy of the Amagá basin is constituted by a lower siliciclastic unit composed of Oligocene quartz-rich continental sediments (alluvial and fluvial deposits with coal intervals) of the Amagá Formation deposited in a strike-slip basin associated with the high obliquity interaction between the Farallon and South-American plates (Silva-Tamayo et al., 2008; Lara et al., 2018). After the Farallon break-up into the Nazca and Cocos plates about ~23 Ma (e.g., Meschede and Barckhausen, 2000; Lonsdale, 2005), there was a change in the Farallon/Nazca kinematics from an oblique to more orthogonal subduction (e.g., Pardo-Casas and Molnar, 1987; Somoza and Ghidella, 2005). This kinematic change of Farallon/ Nazca plates with the South American margin was the precursor of regional discontinuities and changes in the composition from quartz-rich to lithic sandstones of the upper member of the Amagá Formation. Subsequently, during the Early-Middle Miocene, the continental margin of northwestern South America was subjected to the Panamá-Chocó intra-oceanic arc-continent collision (Montes et al., 2015, 2019). The Panamá-Chocó arc formed during the Cretaceous-Eocene due to the north-northwestward subduction of the Farallon plate beneath the Caribbean Plateau (Cardona et al., 2018; León et al., 2018; Barbosa et al., 2019), which collided against northwestern South America as a consequence of the northeastward drift of the Caribbean plate (León et al., 2018; Montes et al., 2015, 2019). This collisional event triggered an orogenic pulse recorded in the cooling histories of exposed rocks along the suture zone, Western Cordillera, and by an unconformity (~13-11 Ma) associated with the tectonic inversion of the Amagá

basin (e.g., Piedrahita et al., 2017; León et al., 2018; Lara et al., 2018). After this collisional episode, the subduction (re)initiation of the buoyant Nazca plate below the South American plate during the Middle-Late Miocene allowed the genesis of the magmatic arc along the suture zone (Rodríguez and Zapata, 2012). Subsequently, the magmatic arc migrated eastward at 5-6° latitude and was positioned in the Amagá basin during the Late Miocene (e.g., Jaramillo et al., 2019; Weber et al., 2020). In this strike-slip hinterland basin, the upper Amagá Formation was overlain and intruded by mafic/intermediate volcanic and subvolcanic bodies with volcaniclastic deposits associated with the Combia and Irra-Tres Puertas formations along the CVP (Fig. 1B). These units are limited by an angular unconformity with the underlying units (e.g., Barroso and Amagá formations) and represent the continental magmatic arc record related to the renewed oblique subduction of the Nazca plate below the South American margin between ~11 and 5 Ma. From Late Miocene to Present-day the Nazca plate geodynamic controls such as oblique subduction (re)initiation, collision/subduction of aseismic ridges (e.g., Sandra ridge), and slab flattening controlled the upper plate architecture and the tectono-magmatic evolution of the continental arc in the northwestern Colombian Andes (e.g., Wagner et al., 2017; Jaramillo et al., 2019; León et al., 2021).

3. Methods

All rocks were collected from three different lava flows that outcrop in the middle part of the Amagá basin (Fig. 1B) and represent the tholeitic suite of the volcanic province.

3.1. Petrography

Thin sections of the samples were made in the TECLAB Gyp S.A. (Bogotá, Colombia). They were later analyzed with a Nikon eclipse 50i pol microscope in the petrography laboratory from the Universidad Industrial de Santander, Colombia, following a grid of 1x1 mm point counting, with 400 points total for each sample. The observed crystals were classified as phenocrysts (>0.5 mm), microphenocrysts (between 0.05 and 0.5 mm), and microcrysts (<0.05 mm), the latter as part of the groundmass, following González (2008). The mineral abbreviations were taken from Siivola and Schmid (2007).

3.2. Mineral chemistry

In situ mineral quantitative analyses (127 for plagioclase and 30 for pyroxene) were performed using a JXA-8530F Field Emission Electron Probe X-ray MicroAnalyzer (FE-EPMA) equipped with 5 wavelength dispersive spectrometers, at the Facility for Analysis, Characterization, Testing and Simulation (FACTS) in Nanyang Technological University (NTU), Singapore. Point analyses were acquired using a focused beam at a probe current of 20 nA and an accelerating voltage of 15 kV. Current was reduced to 10 nA and defocused beam diameters of 3 for analysis of plagioclase, to reduce beam dosage and resultant sodium signal decay. Results were quantified using well characterized natural and synthetic external calibration standards and a ZAF matrix correction procedure. Oxygen content was assumed from cation abundance, with all iron present as Fe²⁺. Error on repeat analysis of standard reference materials was <1% of measured values. Kα X ray lines were monitored for 20-60 s for each element, depending on expected concentrations except for Na Kα which was monitored for only 10 s. Background measurements were performed on either side of each peak position for combined counting times equaling the corresponding peak counting times. Measured peak and background positions were found to be free of interferences within the sample and standard matrices. For this work, it was only used analysis whose sum of the major element oxides was between 97 and 100 wt%. The data was processed for its graphical representation and cation per formula unit calculation, using the GCDkit 4.1 (Janouŝek et al., 2006), CFU and CFU-PINGU (Cortés, 2017) programs.

3.3. Whole rock chemistry

Whole-rock analyses (major and trace elements) were made with the ICP-OES (Inductively coupled plasma optical emission spectrometry) and ICP-MS (Inductively Coupled Plasma mass spectrometry) techniques, in the ActLabs laboratories (Colombia). Major oxides are reported in weight percentage (wt%) and trace elements in parts per million units (ppm). The loss of ignition (LoI) was calculated from the weight of the samples, and the iron was reported as Fe₂O₃ total. The results were plotted using the GCDkit 4.1 (Janouŝek *et al.*, 2006) software.

4. Results

4.1. Petrography and mineral chemistry

The studied rocks are hypocrystalline with porphyritic textures. They have pheno- and microphenocrysts (varying between 26.0 to 29.0 vol.%) of plagioclase and clinopyroxene embedded in a microcrystalline and glassy groundmass (61.0-63.0 vol.%) (Table 1; Fig. 2A). Clinopyroxene phenocrysts are absent in sample IIES-V-019 (Table 1). The glassy zones vary between 9.5 and 23.0 vol.%, and the microcrystalline groundmass hosts plagioclase (24.6-35.8 vol.%) and clinopyroxene microcrysts (14.1-18.7 vol.%) in all rocks. Plagioclase is the most abundant mineral phase in all samples, and it appears as subhedral to euhedral phenocrysts (10.0-13.4 vol.%) and microphenocrysts (14.6-17.0 vol.%) (Fig. 2B), occasionally displaying glomeroporphyritic texture (Fig. 2C, D). Some plagioclase crystals exhibit sieve texture (Fig. 2A, B, D, E), embayment and dissolution rim (Fig. 2A, D),

TABLE 1. PETROGRAPHIC ANALYSIS OF THE STUDIED SAMPLES.

				Mineral	ogy(%))		Crystals	(Groundr	nass
Sample	Coordinates		Pl		(Срх		(%)		(%)	
		Ph	Mph	Mc	Ph	Mp	Mc	Ph+Mph	Mc	glass	oxides
IIES-V-018	5°35'30" N 75°47'09" W	13.4	14.6	24.6	-	0.25	16	28.25	40.6	23	8.15
IIES-V-019	5°35'53" N 75°47'15" W	10.3	15.75	35.8	-	-	18.75	26	53.5	9.5	11
IIES-V-020	5°43'39" N 75°48'46" W	10	17	26	0.5	1.2	14.1	28.7	40.1	21.2	10

Pl: plagioclase, Cpx: clinopyroxene, Ph: phenocryst, Mph: microphenocryst, Mc: microcryst.

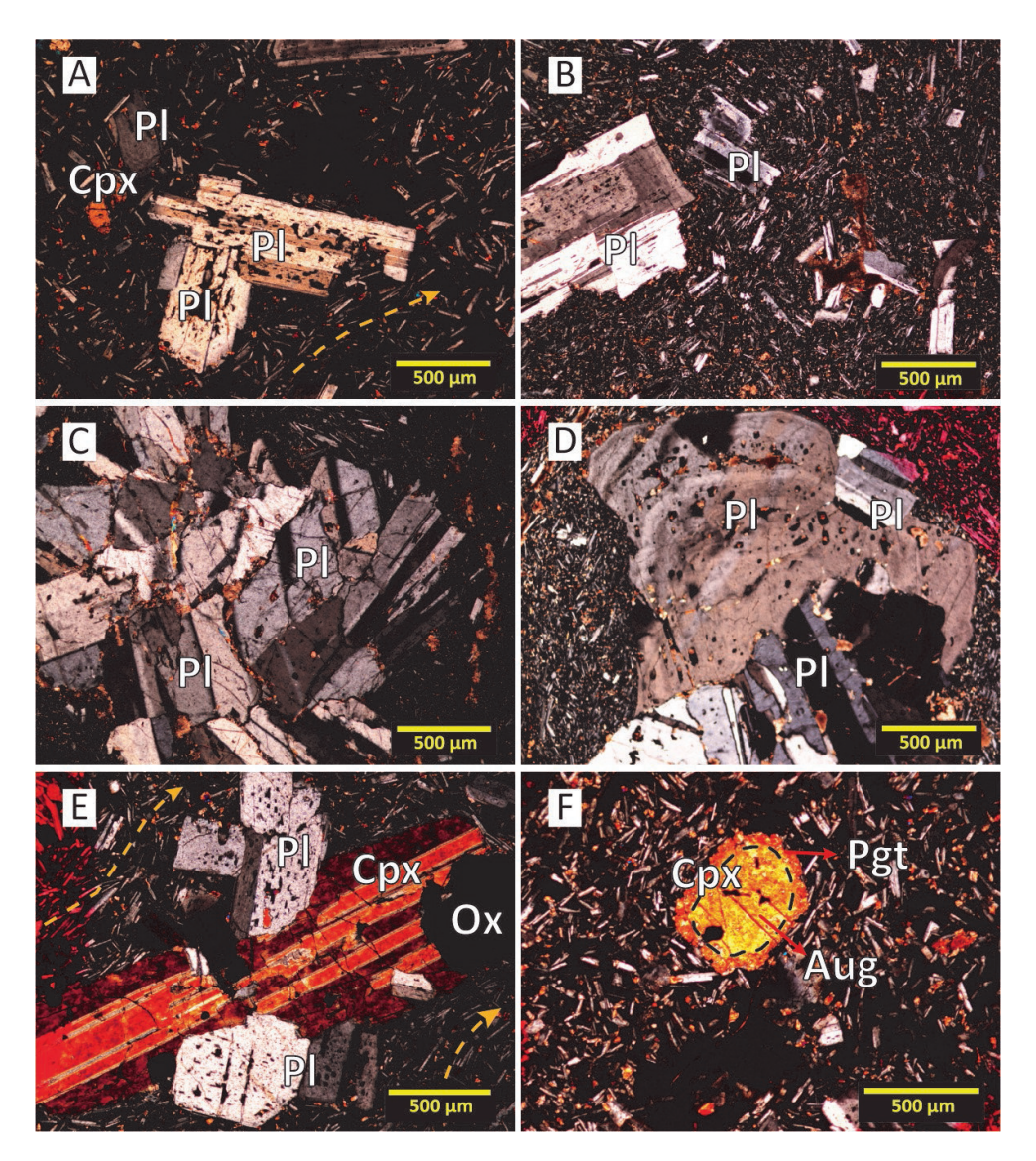


FIG. 2. A. Plagioclase pheno- and microphenocrysts and clinopyroxene microphenocrysts, in a microcrystalline groundmass with glassy zones (IIES-V-020 sample). B. Plagioclase phenocryst with albite twinning, zoning and sieve texture in its core, and euhedral plagioclase microphenocrysts (IIES-V-019 sample). C. Plagioclase glomerocrysts with sieve texture, albite and pericline twinning (IIES-V-018 sample). D. Plagioclase glomerocrysts with sieve texture, dissolution rims, albite twinning and zoning (IIES-V-019 sample). E. Plagioclase with sieve texture, clinopyroxene with polysynthetic twinning, and Fe-Ti oxide glomerocrysts in groundmass with fluidal texture (indicated by the dotted arrows) (IIES-V-020 sample). F. Clinopyroxene phenocrysts with coronitic texture, in groundmass with intersertal texture (IIES-V-020 sample). Pl: plagioclase, Cpx: clinopyroxene, Aug: augite, Pgt: pigeonite, Ox- Fe-Ti oxide. All photomicrographs were taken in crossed Nichols.

as well as zoning (Fig. 2B, D) and albite and pericline twinning. Clinopyroxene phenocrysts (0.5 vol.%) are only found in the sample IIES-V-020, while microphenocrysts are present in samples IIES-V-018 and IIES-V-020 (0.2-1.2 vol.%, respectively) (Table 1). Clinopyroxene also forms

glomeroporphyritic texture with plagioclase and some phenocrysts show polysynthetic twinning (Fig. 2E) and coronitic texture (Fig. 2F). All rocks display fluidal textures, recognized by microcrysts oriented around phenocrysts (Fig. 2E) and also intersertal textures (Fig. 2F).

Compositionally (Table 2; Supplementary material 1), the plagioclase phenocrysts range from labradorite to anorthite (An_{56} - An_{90} ; Fig. 3A). The sample IIES-V-018 shows a more discrete range of compositions (An_{69} - An_{83}), whereas the sample

IIES-V-020 displays a wider range $(An_{56}-An_{90})$. The plagioclase microphenocrysts display a range between andesine and bytownite $(An_{50}-An_{84}; Fig. 3B)$. Samples IIES-V-018 and IIES-V-019 show a nearly identical range of compositions $(An_{58}-An_{82})$, while

TABLE 2. REPRESENTATIVE ANALYSES OF THE MINERAL PHASES ADDRESSED FOR THE COMBIA VOLCANIC PROVINCE.

		Plagioclase Phenocry			_	Clinopyroxene		Microphenocrysts				
Mineral	P	henocrys	ts	Mic	rophenoci	rysts	Core Augite	Rim Augite	Core	Rim Pigeonite	Augita	Pigeonite
Sample	IIES- V-018	IIES- V-019	IIES- V-020	IIES- V-018	IIES- V-019	IIES- V-020				·V-020		
Code	C1a_1	C4c	C6a_2	C4e	C1b	C3a	C3g_1	C3j_2	C4m_1	C4l_2	C4b	C8i
wt%	-	-										
SiO_2	50.76	48.53	49.59	48.37	47.40	52.00	50.75	51.03	50.52	50.31	50.45	50.74
${\rm TiO}_2$	-	-	-	-	-	-	0.43	0.33	0.40	0.17	0.46	0.27
Al_2O_3	30.46	30.88	30.66	30.88	32.13	29.76	1.43	1.20	2.03	0.67	2.24	0.76
FeO _t	-	-	-	-	-	-	14.94	15.71	13.02	27.17	13.37	24.84
MnO	-	-	-	-	-	-	0.63	0.66	0.47	0.96	0.48	0.98
MgO	-	-	-	-	-	-	12.62	11.81	14.06	15.57	14.02	16.76
CaO	14.53	15.16	14.69	15.09	16.29	13.52	18.81	18.79	18.22	4.29	17.83	4.65
Na ₂ O	3.03	2.90	3.31	2.98	2.20	3.90	0.22	0.26	0.29	0.08	0.24	0.07
K_2O	0.20	0.18	0.17	0.12	0.12	0.22	-	-	-	-	-	-
TOT	98.98	97.64	98.41	97.4	98.1	99.4	99.83	99.79	99.02	99.23	99.10	99.08
Cations	per form	ula unit										
Si	2.33	2.27	2.30	2.27	2.21	2.38	1.94	1.96	1.93	1.97	1.92	1.97
Ti	-	-	-	-	-	-	0.01	0.01	0.01	0.00	0.01	0.01
$Al^{\rm IV}$	-	-	-	-	-	-	0.06	0.04	0.07	0.03	0.08	0.03
$Al^{\rm VI}$	-	-	-	-	-	-	0.01	0.01	0.02	0.00	0.02	0.00
Al^{Tot}	1.65	1.70	1.68	1.71	1.77	1.60	0.06	0.05	0.09	0.03	0.10	0.03
Fe^{+2}	-	-	-	-	-	-	0.05	0.03	0.05	0.03	0.04	0.02
Fe^{+3}	-	-	-	-	-	-	0.43	0.47	0.36	0.86	0.38	0.78
Fe^{Tot}	-	-	-	-	-	-	0.48	0.50	0.42	0.89	0.43	0.80
Mn	-	-	-	-	-	-	0.02	0.02	0.02	0.03	0.02	0.03
Mg	-	-	-	-	-	-	0.72	0.68	0.80	0.91	0.80	0.97
Ca	0.72	0.76	0.73	0.76	0.82	0.66	0.77	0.77	0.74	0.18	0.73	0.19
Na	0.27	0.26	0.30	0.27	0.20	0.35	0.02	0.02	0.02	0.01	0.02	0.01
K	0.01	0.01	0.01	0.01	0.01	0.01	-	-	-	-	-	-
Sum	4.98	5.01	5.02	5.02	5.00	5.00	4.02	4.01	4.03	4.02	4.02	4.01
$\boldsymbol{X}_{\!\scriptscriptstyle{An}}$	72	74	70	73	80	65	-	-	-	-	-	-
Mg#	-	-	-	-	-	-	60	57	66	51	65	55

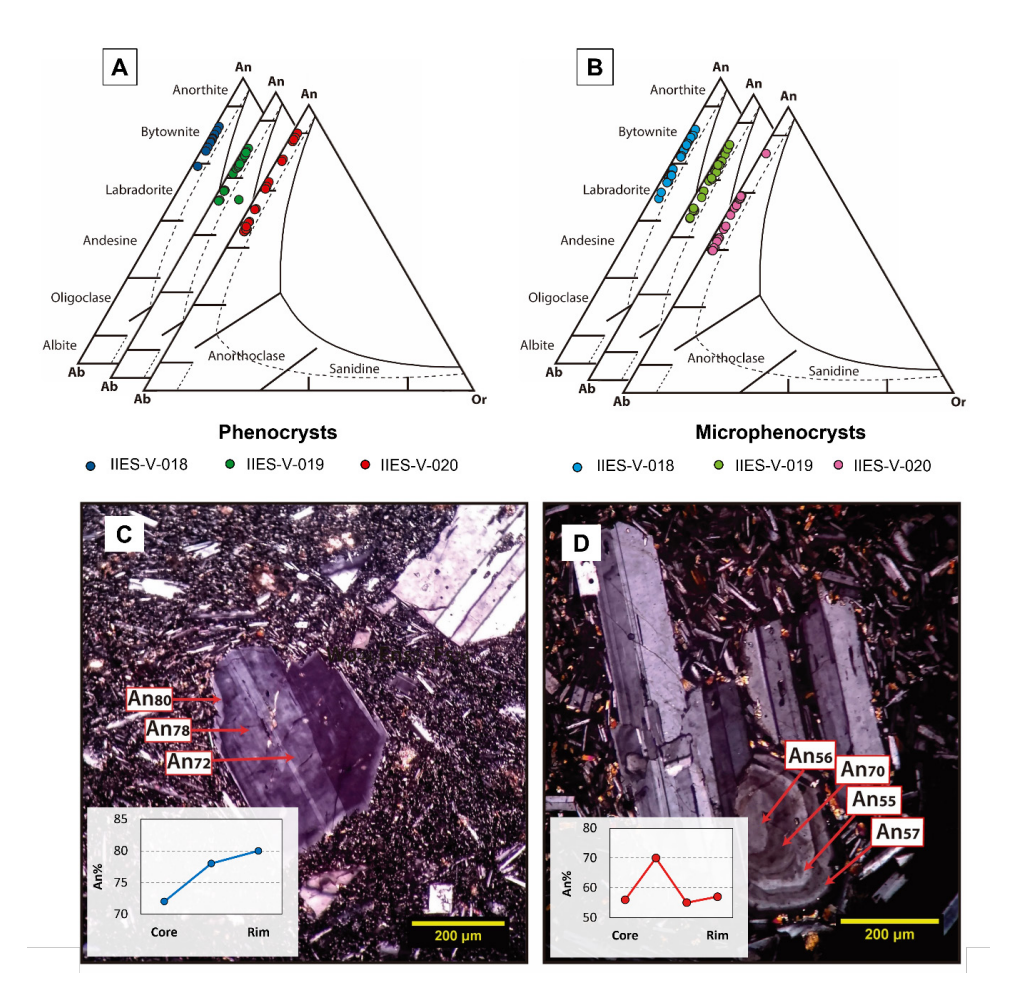


FIG. 3. Ternary classification diagram Ab-An-Or for feldspar (Deer *et al.*, 1992). A. Plagioclase phenocrysts. B. Plagioclase microphenocrysts. C. Inverse zoning in sample IIES-V-018, crossed Nichols. D. Oscillatory zoning in sample IIES-V-020, crossed Nichols. An: anorthite, Ab: albite, Or: orthoclase.

sample IIES-V-020 shows microphenocryts of more intermediate composition (An₅₀-An₆₉), with exception of one crystal that falls within the bytownite field (An₈₄). The compositional analysis from core to rim in the minerals also evidence the previously identified inverse (Fig. 3C) and oscillatory zoning (Fig. 3D) in all samples. The pyroxene phenocrysts of sample IIES-V-020 (Table 1, Fig. 4A) are classified as augite (Wo₄₂₋₃₇, Ens₄₂₋₃₅, Fs₂₆₋₁₈; Fig. 4B), a few of which show pigeonite rims (Wo₁₀₋₉, Ens₄₉₋₄₆, Fs₄₅₋₄₁; Fig. 4C). Similar range of compositions are observed, augite (Wo₃₉₋₃₅, Ens₄₂₋₃₈, Fs₂₇₋₂₀) and pigeonite (Wo₁₃₋₉, Ens₄₉₋₄₄, Fs₄₃₋₄₁), for the microphenocrysts of sample IIES-V-020. Unfortunately, no microphenocrysts of sample IIES-V-018 yielded truthful results.

4.2. Geochemistry

Compositionally (Table 3), the studied rocks range from basaltic andesite to andesite, with sample IIES-V-019 being the least evolved of the set (Fig. 5A). They have tholeitic affinity (Fig. 5B) and present a K content (Fig. 5C) that range from medium (IIES-V-019) to high (IIES-V-018 and IIES-V-020). If compared with tholeitic samples from previous studies (Marriner and Millward, 1984; Borrero and Toro-Toro, 2016; Jaramillo *et al.*, 2019), samples IIES-V-018 and IIES-V-020 show the more evolved compositions and the highest K content (Fig. 5C). The sample IIES-V-019 falls within the range of compositions displayed by other studies. Variation

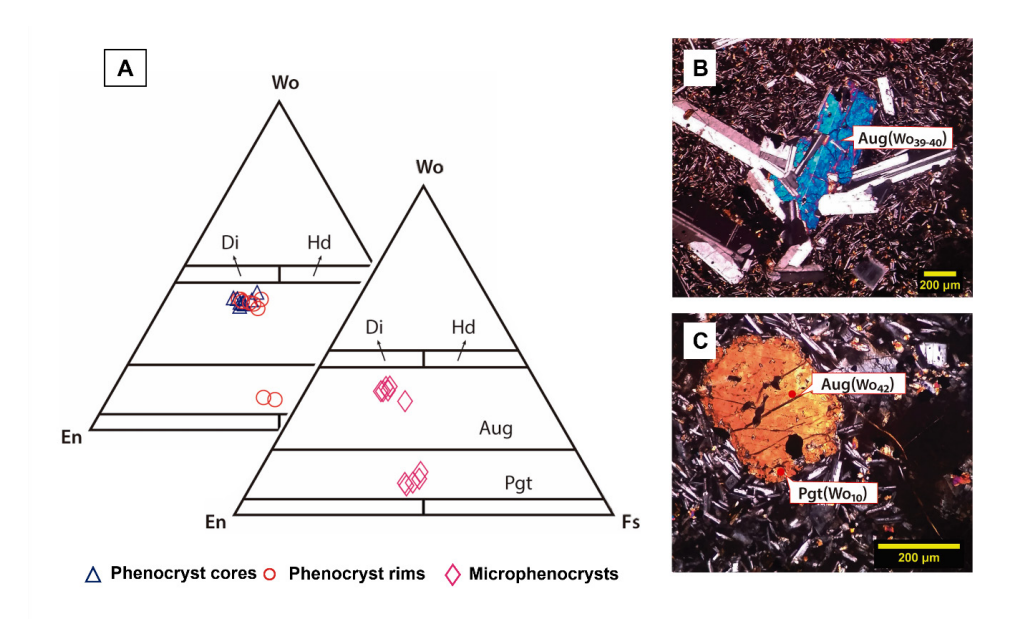


FIG. 4. A. Classification diagram of pyroxene composition (Morimoto, 1989) (IIES-V-020 sample). Note that phenocrysts were analyzed at cores and rims, while microphenocrysts only at a single spot. B. Homogeneous composition augite, crossed Nichols.
C. Augite crystal with pigeonite rim, crossed Nichols. Wo: wollastonite, Di: diopside, Hd: hedenbergite, Aug: augite, Pgt: pigeonite, En: enstatite, Fs: ferrosilite.

TABLE 3. MAJOR (WT%) AND TRACE (PPM) ELEMENTS CHEMICALANALYSES FOR THE COMBIA VOLCANIC PROVINCE.

Sample	IIES-V-018	IIES-V-019	HES-V-020 5°43'39" N		
	5°35'30" N	5°35'53" N			
	75°47'09" W	75°47'15" W	75°48'46" W		
Major oxides					
SiO_2	57.37	52.79	57.72		
Al_2O_3	16.74	16.41	15.88		
$Fe_2O_3(T)$	9.27	11.39	10.84		
MnO	0.20	0.18	0.21		
MgO	1.78	2.92	1.80		
CaO	6.53	8.30	6.34		
Na ₂ O	3.31	3.01	3.29		
K,O	2.20	1.50	2.22		
TiO ₂	0.79	1.14	0.76		
P_2O_5	0.45	0.42	0.47		
LOI	1.87	2.15	0.66		
Total	100.5	100.2	100.2		

table 3 continued.

Sample	IIES-V-018	IIES-V-019	HES-V-020 5°43'39" N 75°48'46" W		
_	5°35'30" N	5°35'53" N			
	75°47'09" W	75°47'15" W			
race elements					
Be	1	-	1		
V	120	291	122		
Ba	1,038	1,060	1,021		
Sr	496	477	477		
Y	27	19	24		
Zr	90	72	89		
Cr	70	70	180		
Co	21	26	21		
Cu	120	160	130		
Zn	110	110	100		
Ga	18	19	18		
Ni	<20	<20	<20		
Ge	2	2	2		
As	6	16	7		
Rb	40	38	46		
Nb	4	3	4		
Sn	1	1	1		
Sb	0.8	6.4	1.2		
Cs	0.8	15.5	1.1		
La	11.1	8.5	10.2		
Ce	22.9	17.8	21.3		
Pr	3.16	2.51	2.93		
Nd	14.3	11.7	13.7		
Sm	3.9	3.1	3.7		
Eu	1.23	1.06	1.17		
Gd	4.6	3.7	4.3		
Tb	0.8	0.6	0.7		
Dy	4.7	3.8	4.3		
Но	1	0.8	0.9		
Er	3	2.2	2.6		
Tm	0.44	0.33	0.38		
Yb	3	2.1	2.5		
Lu	0.47	0.34	0.38		
Hf	2.8	2.1	2.5		
Ta	0.3	0.3	0.3		
Ti	-	0.5	0.1		
Pb	7	9	8		
Th	2	1.5	1.9		
U	0.9	0.8	0.9		
aEu/Eu*	0.88	0.95	0.89		

^a Eu/Eu*=Eu_N/[(Sm_N× Gd_N)]^{1/2}. \mathbf{X}_N : normalized to primitive mantle values in Sun and McDonough (1989).

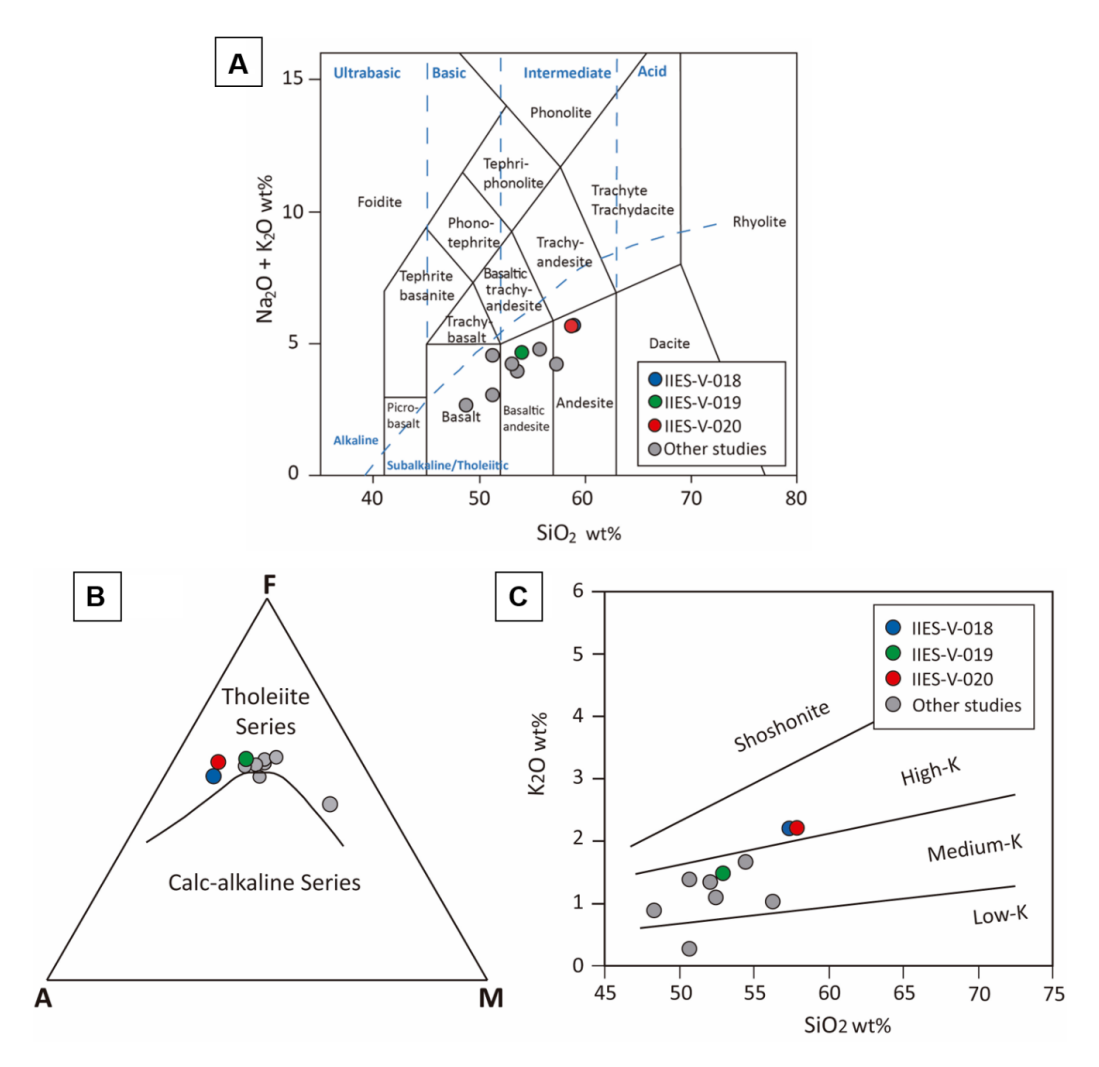


FIG. 5. A. Silica versus Alkali variation diagram (TAS- Le Bas *et al.*, 1986). **B.** Alkali (Na₂O+K₂O)-FeO- MgO variation diagram (AFM- Irvine and Baragar, 1971). **C.** SiO₂ versus K₂O variation diagram (Gill, 1981). Gray points correspond to the tholeiitic lava flows studied by Marriner and Millward (1984), Borrero and Toro-Toro (2016) and Jaramillo *et al.* (2019).

diagrams of major and trace elements versus SiO_2 (Fig. 6), for the tholeiitic rocks of the CVP (this study and others: Marriner and Millward, 1984; Borrero and Toro-Toro, 2016; Jaramillo *et al.*, 2019) shows negative correlations for CaO and MgO, and positive for Th and Nb, and crudely for Rb.

The behavior of trace elements normalized to primitive mantle (Fig. 7A) is similar for the three studied samples, with a relative enrichment in large ion lithophile elements (LILE) and negative anomalies of Th, Nb, Ta, Zr and Ti, and positive anomalies of Ba, K, Pb, Sr and P. Such behavior is also observed in other tholeiitic rocks of the province

(Marriner and Millward, 1984; Borrero and Toro-Toro, 2016; Jaramillo *et al.*, 2019). The rare earth elements diagram (REE; Fig. 7B) also shows a similar behavior between the studied samples, with a slight light REE enrichment (LREE) and a minor Eu negative anomaly (Eu/Eu*<1). Discrimination diagrams show how, if compared with previous studies (Marriner and Millward, 1984; Borrero and Toro-Toro, 2016; Jaramillo *et al.*, 2019), these samples exhibit a slight enrichment, especially in the LREE. The discrimination diagram La/Yb versus Th/Nb (Fig. 7C) show that the samples plot within the continental arc field.

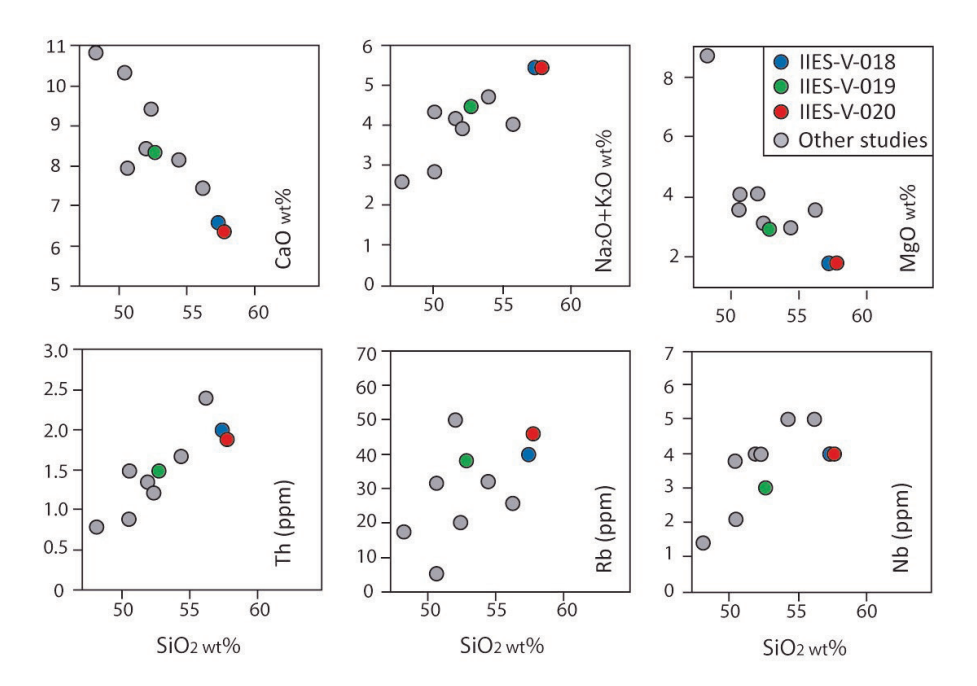


FIG. 6. Silica (SiO₂) versus major and trace elements variation diagrams. Gray points correspond to the tholeiitic lava flows studied by Marriner and Millward (1984), Borrero and Toro-Toro (2016) and Jaramillo *et al.* (2019).

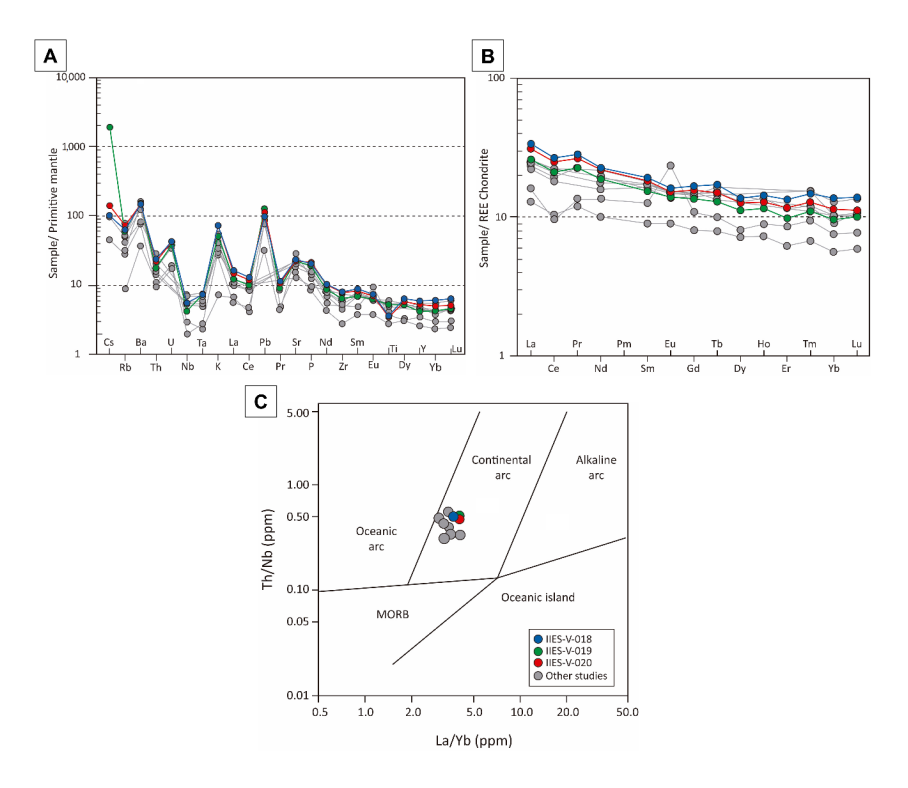


FIG. 7. A. Multielement diagram normalized to primitive mantle (Sun and McDonough, 1989). B. Rare earth elements diagram normalized to chondrite (Nakamura, 1974). C. La/Yb versus Th/Nb variation diagram (Hollocher *et al.*, 2012). Gray points correspond to the tholeitic lava flows studied by Marriner and Millward (1984), Borrero and Toro-Toro (2016) and Jaramillo *et al.* (2019).

5. Interpretation and discussion

5.1. Magmatic processes identified by rock textures

The textures and compositional variations observed in the minerals of the studied rocks (Fig. 8) have allowed us to propose four main processes that underwent by the magma during stagnation and ascent.

Physical and chemical changes in the magmatic reservoir. This is evidenced by the embayment and sieve textures in plagioclase crystals linked to dissolution (Fig. 8A, B). Thermodynamic changes cause disequilibrium between crystals and melt, which triggers the dissolution inside the crystals and/or in their surfaces (Tsuchiyama, 1985; Nelson and Montana, 1992; Tepley *et al.*, 1999; Couch *et al.*, 2001; Monfaredi *et al.*, 2009; Ustunisik *et al.*, 2014).

Rapid decompression. It is evidenced by the presence of sieve texture cores in plagioclase, with rims lacking dissolution zones (Fig. 8B). In addition to physical and chemical changes previously mentioned, rapid decompression during magma ascent followed by new equilibrium conditions allows the subsequent formation of rims, which do not evidence internal dissolution (Nelson and Montana, 1992; Seaman, 2000; Monfaredi *et al.*, 2009).

Convective movements. They are interpreted from oscillatory zoning in plagioclase crystals (Fig. 8A) and the development of glomeroporphyritic texture (Fig. 8C, D). Convective movements during magma ascent generate perturbation and turbulence that cause local variations in the melt conditions, leading to the development of zoning depending on the crystal location: higher An zones are developed in hotter melt parts, while lower An zones are developed in colder parts (Pearce and Kolisnik, 1990; Shcherbakov

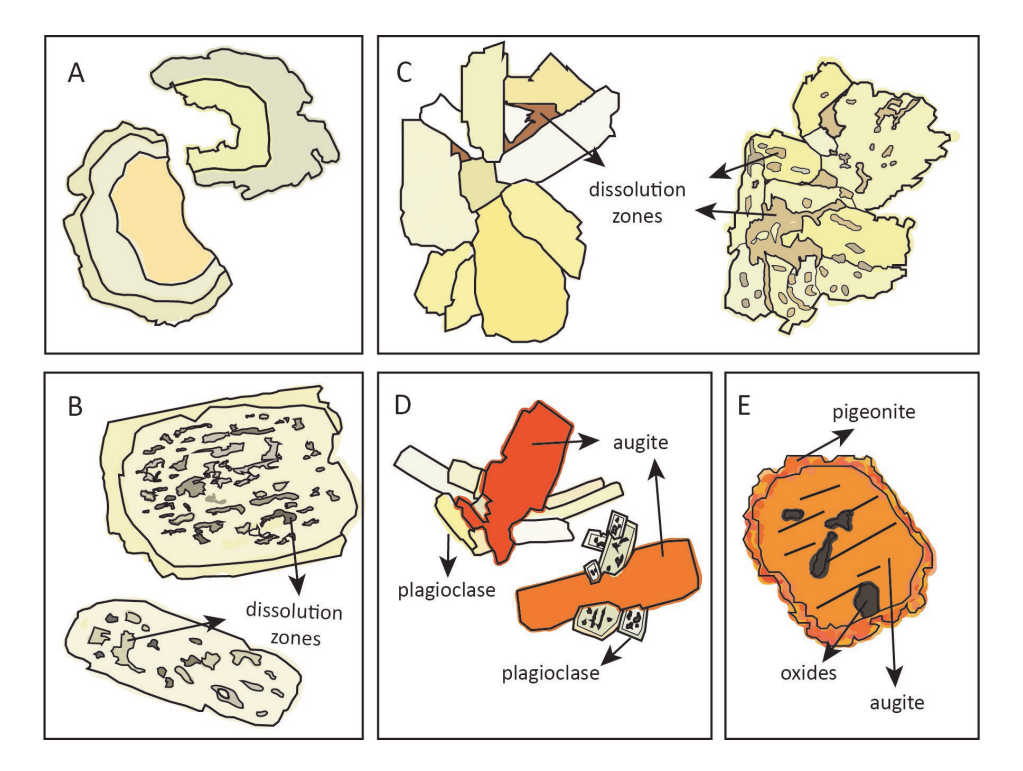


FIG. 8. Sketches used to illustrate the features that allowed us to propose the main processes that underwent the magma during stagnation and ascent. A. Anhedral plagioclase crystals with dissolution (embayment texture). Many crystals also exhibit oscillatory and inverse zoning. B. Euhedral to subhedral plagioclase crystals with sieve texture cores in addition to sane rims. C. Glomerocrysts formed by euhedral to subhedral plagioclase crystals, and by anhedral to subhedral plagioclase crystals with sieve texture and reaction rims. D. Glomerocrysts of euhedral augite crystals with euhedral plagioclase crystals, some of them with sieve texture. E. Subhedral augite crystals with pigeonite rims (i.e., coronitic texture).

et al., 2011; Murcia and Németh, 2020). Furthermore, convective movement is a key factor to group together crystals with or without dissolution. Several crystal planes get chemically isolated from the system's melt, leading the melt that got trapped between the crystals to eventually cool down and couple them (Vance, 1969; Hogan, 1993). The resulting glomerocrysts are usually located along the chilled margins and will finally get removed and incorporated into the ascending magma (Jeffery et al., 2013).

Mixing processes. Mixing produced by magmatic recharge is evidenced by Mg-rich (*i.e.*, pigeonite; Fig. 8E) rims on augite crystals. The injection of a hotter magma causes disequilibrium and changes in temperature, pressure and H₂O content, leading to the development of new mineral phases (Couch *et al.*, 2001; Shcherbakov *et al.*, 2011).

5.2. Crystallization conditions

Geothermobarometry analyses presented here correspond to crystal-liquid chemical relations, where the whole-rock composition represents the melt in which the minerals crystallized. To reproduce the composition where the crystals formed based on partition coefficients, plagioclase phenocrysts were compared to the least evolved rock (SiO₂=52.79 wt%), while the microphenocrysts were compared to the most evolved rock (SiO₂=57.72 wt%); this assuming that microphenocrysts crystallized later, given the predominance of a less An content in their composition. Also, pyroxene phenocrysts cores (augite) were compared to the least evolved rock (SiO₂=52.79 wt%), while the phenocrysts rims (augite and occasionally pigeonite) were compared to the most evolved rock (SiO₂=52.79 wt%), assuming that rims should have crystallized later in a more evolved magma than cores. Based on the above, the exchange coefficient (K_D) between crystals, and melt (plagioclase: 0.27±0.11; clinopyroxene: 0.28±0.080; Putirka, 2008) allowed equilibrium determination to reproduce reliable crystallization conditions (Table 3; Supplementary material 2).

According to the equilibrium relation, 56 out of 127 plagioclase crystals, 14 out of 25 augite crystals and 7 out of 7 pigeonite crystals met the requirement for applying the geothermobarometers. Then, Eq. 24a and 25a of Putirka (2008) were applied for the plagioclase, and Eq. 32d and 32a of Putirka (2008) were applied for the pyroxene. Here

it is important to mention that the clinopyroxene thermometer includes the liquid composition, but the barometer is based exclusively on the mineral composition. Errors estimated by Putirka (2008) for temperature and pressure equations mentioned are ± 52 °C and ± 0.1 GPa. The initial water content value (H₂O wt%) required to apply the plagioclase geothermobarometric equation was assumed as 1.5 wt%, considering that Zimmer *et al.* (2010) reports that water content in tholeitic magmas is close but less than 2.0 wt%. Finally, depth was estimated from the pressure values calculated, assuming an average density of the continental crust of 2.7 g/cm³, which corresponds to a geobaric gradient of ~27 MPa/km (Best, 2003).

As a whole, results show that plagioclase crystallized at a temperature range between 1,095 and 1,153 °C, and pressures of 0.22 to 0.60 GPa, which corresponds to depths between 8 and 23 km (Fig. 9). Phenocrysts were formed between 13 and 23 km depths, while microphenocrysts crystallization took place between 8 and 19 km depths. Augite crystals were formed in a temperature range between 1,046 and 1,131 °C, and pressures of 0.09 to 0.21 GPa, which corresponds to depths between 3 and 8 km, being the microphenocrysts the ones that evidence the lowest temperature values. Pigeonite microphenocrysts were formed in a temperature range between 867 and 1,039 °C, and pressures of 0.40 to 0.60 GPa, which corresponds to depths between 6 and 23 km. Augite shows temperature and pressure decreasing from cores to rims, which indicates growth during the magma ascent. Pigeonite rims on augite crystals (i.e., coronitic texture), results show lower temperatures in rims (e.g., 1,039-963 °C), but surprisingly higher pressure and depth of crystallization (0.38 GPa and 14 km, respectively); this occurs due to the higher MgO content, which it is interpreted as as related to a heterogeneous melt instead of a deeper formation. Rather, these rims formation are associated with the magma ascent dynamics, but also with the magmatic recharge or mixing and its subsequent cooling. From petrographic analyses, these processes were evidenced and then related to compositional differences.

In summary, both the mineralogy and crystallization conditions found in the analyzed samples indicate that the mineral formation in the tholeiitic products took place at less than 23 km depth (plagioclase, augite and pigeonite), and continued their formation during ascent until they reached a depth of 3 km.

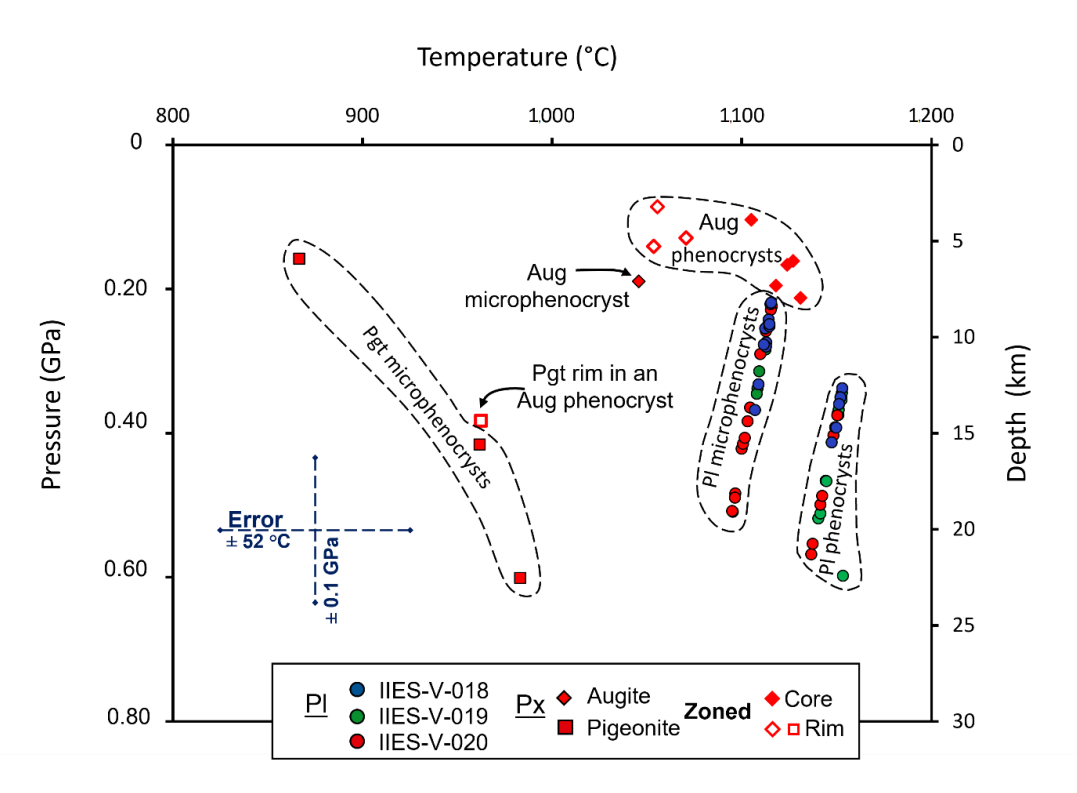


FIG. 9. Pressure (and depth) versus Temperature diagram, which illustrates crystallization conditions for the studied plagioclase and pyroxene pheno- and microphenocrysts. Pl: plagioclase, Px: pyroxene, Aug: augite, Pgt: pigeonite.

5.3. Geochemical processes

The tholeiitic lava flows analyzed in this study, together with the previously reported samples (Marriner and Millward, 1984; Tejada *et al.*, 2007; Borrero and Toro-Toro, 2016; Jaramillo *et al.*, 2019), evidence a basaltic and andesitic composition in the CVP. Negative trends in CaO, MgO, FeO and TiO₂ (these last two not shown) vs. SiO₂ (Fig. 8), indicate calcic pyroxene (augite) and plagioclase fractionation, as supported by the textural and geothermobarometric analyses. The slightly negative Eu (Eu/Eu*) anomaly is also evidence of the fractionation process.

LREE (Fig. 7B) enrichment and La/Yb vs. Th/Nb (Fig. 7C) relations presented by the products clearly show that rocks were formed in a continental subduction arc (Gorton and Schlandl, 2000). LILE incompatible elements enrichment compared to the HFSE (Fig. 7A) suggests possible crustal contamination processes occurred during the magma stagnation or ascent through the crust (*e.g.*, Sosa-Ceballos *et al.*, 2021). This assimilation has

already been suggested in previous studies (*e.g.*, Jaramillo *et al.*, 2019; Weber *et al.*, 2020; Santacruz *et al.*, 2021).

5.4. Magmatic system and tectonic implications

The magmatic system associated with the tholeiitic lava flows from the CVP is part of a continental volcanic arc (Fig. 10), which is characterized for showing conditions of evolution related to magmatic differentiation by fractional crystallization, assimilation and magma mixing processes. However, the mafic composition suggests that the magmatic system, which allowed the releasing of tholeitic products, was not constituted by long-term magma stagnation zones. Thus, magmatic evolution can be linked to a relative rapid ascent of melt associated with the kinematics related to the development of the strike-slip hinterland Amagá basin due to the Panamá-Chocó intra-oceanic arc-continent collision (Montes et al., 2015, 2019). Then, magma evolution was controlled by crystallization of plagioclase and clinopyroxene (augite and pigeonite) en route (Fig. 11).

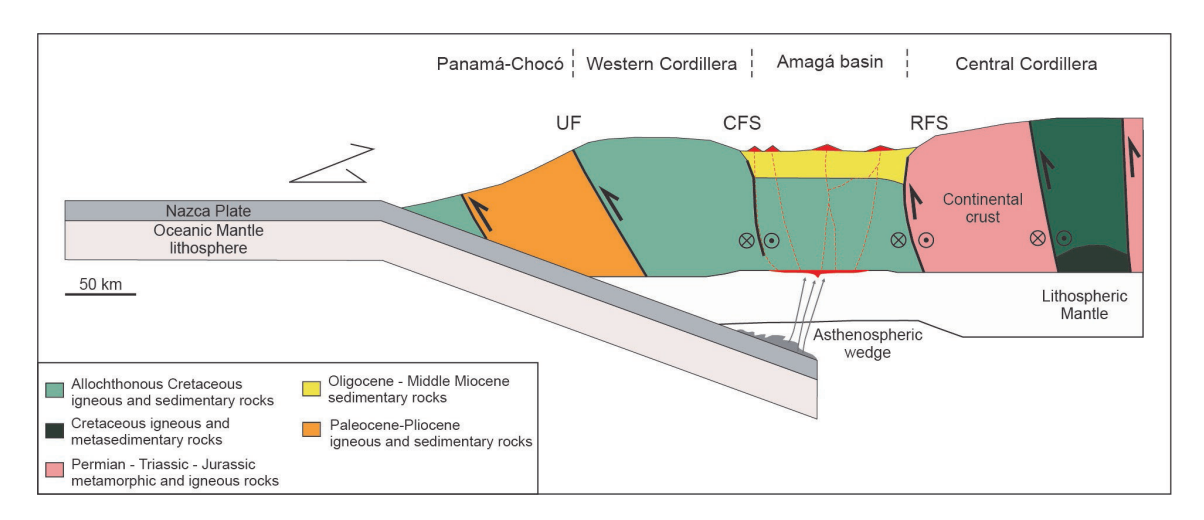


FIG. 10. Simplified geodynamic model of the Colombian Andes at 5° N during the Late Miocene (~11 - 9 Ma), and the Combia Volcanic Province location in the Amagá basin. UF: Uramita Fault, CFS: Cauca Fault System, RFS: Romeral Fault System.

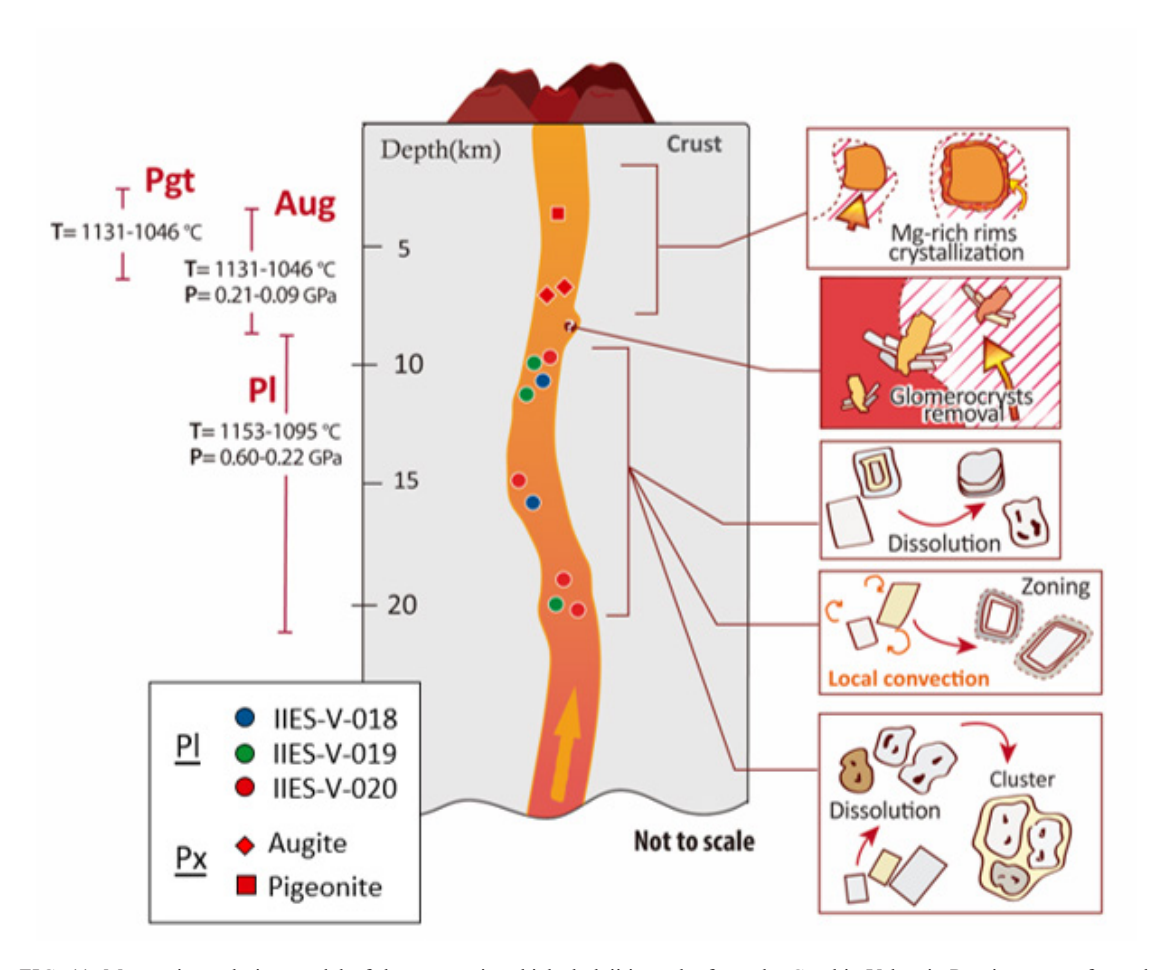


FIG. 11. Magmatic evolution model of the system in which tholeiitic rocks from the Combia Volcanic Province were formed. **Pgt:** pigeonite, **Aug:** augite, **Pl:** plagioclase.

Specifically, at 23 km deep, magma temperature was around 1,150 °C (melting occurred at approximately 1,200 °C; cf. Lee et al., 2009), however the magma reached the surface at ~860 °C. Pressure conditions extracted from the different mineral phases, in addition to the textural characteristics described and the magmas compositional evolution, allow us to propose the occurrence of some typical magmatic differentiation processes mentioned before, and local convective movements related to mineral thermodynamic disequilibrium and heterogeneities in the melt composition, such as oscillatory zoning and reaction rims. These local convective movements can also be related to relatively short stagnation zones, where crystals clustered together (glomeroporphyritic texture) that were later disturbed by the magma ascent itself or even by episodic magmatic recharges (Seaman, 2000).

These results add to the ideas proposed by Weber et al. (2020), who analyzed the calc-alkaline products from the amphibole and garnet crystals composition. Therefore, it is possible to suggest that the tholeiitic products were formed by a magma that suffered a relatively rapid ascent involving plagioclase and clinopyroxene fractional crystallization with only shorttime stagnation zones. In contrast, the calc-alkaline products were the consequence of differentiation linked to crustal assimilation and crystallization of mostly amphibole, but also surely Fe and Ti oxides, from magmas (tholeiitic?) stagnated firstly at depths close to 20 km. Garnet formation allows the adakiticlike signature development (Weber et al., 2020). This scenario can be extrapolated to the entire magmatism and can be considered as an alternative one to the crust local variations (thinning) model (cf. Jaramillo et al., 2019) or a mixture of materials in the magma origins (cf. Bernet et al., 2020) to explain the typical compositional variation in the CVP.

6. Conclusions

The tholeiitic lava flows that gave origin to the CVP, consist mainly in plagioclase crystals of labradorite and bytownite composition, and clinopyroxene of augite and pigeonite composition. These minerals can be found in clusters, with zoning, sieve texture and/or reaction rims.

Chemical composition of tholeiitic lava flows indicates a variation between andesite and basaltic andesite. Trace elements distribution patterns, LILE

and LREE enrichment, together with La/Yb versus Th/Nb content also indicate a magmatic system located in a continental arc, affected by crustal contamination processes.

The origin of the CVP is proposed as a relative simple magmatic system, with a relative rapid magma ascent and fractional crystallization dominated by plagioclase, augite and pigeonite; this process allowed the tholeiitic signature in the emitted magma. Subsequent calc-alkaline products are related to the fractional crystallization of other mineral phases (e.g., olivine, amphibole, Fe and Ti oxides, garnet), besides assimilation associated with magma stagnation in the upper crust.

Acknowledgements

This work was supported by the Instituto de Investigaciones en Estratigrafía (IIES) from the Universidad de Caldas, Colombia, and the project 0279918 from the Vicerrectoría de Investigaciones y Posgrados awarded to H. Murcia and A. Pardo. D. Schonwalder was sponsored by MINCIENCIAS Colombia (Posdoctoral Grant No. 848-2019, Code No. 201010028319) at the Universidad de Caldas (Code No. 807040-125-2020). S. Echeverri was sponsored by MINCIENCIAS-ANH-Universidad de Caldas (Posdoctoral Grant No. FP44842-494-2017, Resolution No. H1193). We thank the reviewer B. Godoy for his constructive comments.

Referencias

Barbosa-Espitia, Á.A.; Kamenov, G.D.; Foster, D.A.; Restrepo-Moreno, S.A.; Pardo-Trujillo, A. 2019. Contemporaneous Paleogene arc-magmatism within continental and accreted oceanic arc complexes in the northwestern Andes and Panama. Lithos 348: 105185. doi: https://doi.org/10.1016/j.lithos.2019.105185

Bayona, G.; Cardona, A.; Jaramillo, C.; Mora, A.; Montes, C.; Valencia, V.; Ayala, C.; Montenegro, O.; Ibañez-Mejía, M. 2012. Early Paleogene magmatism in the northern Andes: Insights on the effects of Oceanic Plateaucontinent convergence. Earth and Planetary Science Letters 331: 97-111.

Bernet, M.; García, J.M.; Chauvel, C.; Londoño, M.J.R.; Marín-Cerón, M.I. 2020. Thermochronological, petrographic and geochemical characteristics of the Combia Formation, Amagá basin, Colombia. Journal of South American Earth Sciences 104: 102897.

Best, M.G. 2003. Igneous and Metamorphic Petrology (2nd Edition) Blackwell: 752 p. Malden.

- Bissig, T.; Leal-Mejía, H.; Stevens, R.B.; Hart, C.J. 2017. High Sr/Y magma petrogenesis and the link to porphyry mineralization as revealed by garnet-bearing I-type granodiorite porphyries of the middle Cauca Au-Cu belt, Colombia. Economic Geology 112 (3): 551-568. doi: https://doi.org/10.2113/econgeo.112.3.551
- Borrero, C.; Toro-Toro, L.M. 2016. Vulcanismo de afinidad adaquítica en el miembro inferior de la Formación Combia (Mioceno tardío) al sur de la subcuenca de Amaga, noroccidente de Colombia. Boletín de Geología 38 (1): 87-100.
- Cardona, A.; León, S.; Jaramillo, J.S.; Montes, C.; Valencia, V.; Vanegas, J.; Bustamante, C.; Echeverri, S. 2018. The Paleogene arcs of the northern Andes of Colombia and Panama: Insights on plate kinematic implications from new and existing geochemical, geochronological and isotopic data. Tectonophysics 749: 88-103.
- Cortés, J.A. 2017. CFU-PINGU. https://vhub.org/resources/ cfupingu.
- Couch, S.; Sparks, R.S.J.; Carroll, M.R. 2001. Mineral disequilibrium in lavas explained by convective self-mixing in open magma chambers. Nature 411: 1037-1039.
- Deer, W.; Howie, R.; Zussman, J. 1992. An introduction to the rock-forming minerals. Longman Scientific and Technology: 712 p. Essex.
- Duque-Caro, H. 1990. The Choco Block in the northwestern corner of South America: Structural, tectonostratigraphic, and paleogeographic implications. Journal of South American Earth Sciences 3 (1): 71-84.
- Echeverri, S.; Cardona, A.; Pardo, A.; Monsalve, G.; Valencia, V.A.; Borrero, C.; Rosero, S.; López, S. 2015. Regional provenance from southwestern Colombia fore-arc and intra-arc basins: implications for Middle to Late Miocene orogeny in the Northern Andes. Terra Nova 27 (5): 356-363.
- Gallego-Ríos, A.F.; Pardo-Trujillo, A.; López-Plazas, G.A.; Echeverri, S. 2020. The Morales Formation (new unit): Record of fluvial-lacustrine environments and the beginning of the Miocene explosive volcanism in the Patía Sub-basin (SW Colombia). The Geology of Colombia 3: 395-415.
- Gill, J.B. 1981. Orogenic andesites and plate tectonics. Springer Berlin: 392 p. Heidelberg.
- González, P.D. 2008. Textura de los cuerpos ígneos. *In* Geología de los Cuerpos Ígneos (Llambías, E.J.; editor): 171-197. Buenos Aires.
- Gorton, M.P.; Schandl, E.S. 2000. From continents to island arcs: a geochemical index of tectonic setting for arc-related and within-plate felsic to intermediate

- volcanic rocks. The Canadian Mineralogist 38 (5): 1065-1073.
- Grosse, E. 1926. El Terciario Carbonifero de Antioquia: das Kohlentertiär Antiquias. Reimer/Vohsen: 361 p.
- Hogan, J.P. 1993. Monomineralic glomerocrysts: textural evidence for mineral resorption during crystallization of igneous rocks. The Journal of Geology 101 (4): 531-540.
- Hollocher, K.; Robinson, P.; Walsh, E.; Roberts, D. 2012. Geochemistry of amphibolite-facies volcanics and gabbros of the Støren Nappe in extensions west and southwest of Trondheim, Western Gneiss Region, Norway: a key to correlations and paleotectonic settings. American Journal of Science 312 (4): 357-416.
- Irvine, T.N.J.; Baragar, W.R.A. 1971. A guide to the chemical classification of the common volcanic rocks. Canadian Journal of Earth Sciences 8 (5): 523-548.
- Janoušek, V.; Farrow, C.M.; Erban, V. 2006. Interpretation of whole-rock geochemical data in igneous geochemistry: introducing Geochemical Data Toolkita (GCDkit). Journal of Petrology 47 (6): 1255-1259.
- Jaramillo, J.S.; Cardona, A.; Monsalve, G.; Valencia, V.; León, S. 2019. Petrogenesis of the late Miocene Combia Volcanic complex, northwestern Colombian Andes: Tectonic implication of short term and compositionally heterogeneous arc magmatism. Lithos 330: 194-210.
- Jaramillo, J.M. 1976. Volcanic rocks of the Río Cauca valley, Colombia S.A. Rice University, Houston. Thesis Degree Master of Arts: https://hdl.handle. net/1911/104201
- Jeffery, A.J.; Gertisser, R.; Troll, V.R.; Jolis, E.M.; Dahren, B.; Harris, C.; Tindle, A.G.; Preece, K.; O'Driscoll, B.; Humaidda, H.; Chadwick, J.P. 2013. The preeruptive magma plumbing system of the 2007-2008 dome-forming eruption of Kelut volcano, East Java, Indonesia. Contributions to Mineralogy and Petrology 166 (1): 275-308.
- Lara, M.; Salazar-Franco, A.M.; Silva-Tamayo, J.C. 2018. Provenance of the Cenozoic siliciclastic intramontane Amagá Formation: Implications for the early Miocene collision between Central and South America. Sedimentary Geology 373: 147-162.
- Le Bas, M.J.; Le Maitre, R.W.; Streckeisen, A.; Zanettin, B.; IUGS Subcommission on the Systematics of Igneous Rocks. 1986. A chemical classification of volcanic rocks based on the total alkali-silica diagram. Journal of Petrology 27 (3): 745-750.
- Lee, C.T.A.; Luffi, P.; Plank, T.; Dalton, H.; Leeman, W.P. 2009. Constraints on the depths and temperatures of basaltic magma generation on Earth and other terrestrial planets using new thermobarometers for

- mafic magmas. Earth and Planetary Science Letters 279 (1-2): 20-33.
- León, S.; Cardona, A.; Parra, M.; Sobel, E.R.; Jaramillo,
 J.S.; Glodny, J.; Valencia, V.A.; Chew, D.; Montes, C.;
 Posada, G.; Monsalve, G.; Pardo-Trujillo, A. 2018.
 Transition from collisional to subduction-related regimes: An example from Neogene Panama-Nazca-South America interactions. Tectonics 37 (1): 119-139.
- León, S.; Monsalve, G.; Jaramillo, C.; Posada, G.; de Miranda, T.S.; Echeverri, S.; Valencia, V.A. 2021. Increased megathrust shear force drives topographic uplift in the Colombian coastal forearc. Tectonophysics 820: 229132.
- Lonsdale, P. 2005. Creation of the Cocos and Nazca plates by fission of the Farallon plate. Tectonophysics 404 (3-4): 237-264.
- López, A.; Sierra, G.M.; Ramírez, D.A. 2006. Vulcanismo neógeno en el suroccidente antioqueño y sus implicaciones tectónicas. Boletín de Ciencias de la Tierra 19: 27-42.
- Marriner, G.F.; Millward, D. 1984. The petrology and geochemistry of Cretaceous to Recent volcanism in Colombia: the magmatic history of an accretionary plate margin. Journal of the Geological Society 141 (3): 473-486.
- Meschede, M.; Barckhausen, U. 2000. Plate tectonic evolution of the Cocos-Nazca spreading center. *In* Proceedings of the ocean drilling program, scientific results 170, College Station, Tex.: Ocean Drilling Program No. 10: 10 p.
- Monfaredi, B.; Masoudi, F.; Tabakh, S.A.; Shaker, A.F.; Halama, R. 2009. Magmatic interaction as recorded in texture and composition of plagioclase phenocrysts from the Sirjan area, Urumieh-Dokhtar magmatic arc, Iran. Journal of Sciences, Islamic Republic of Iran 20 (3): 243-251.
- Montes, C.; Cardona, A.; Jaramillo, C.; Pardo, A.; Silva,
 J.C.; Valencia, V.; Ayala, C.; Pérez-Ángel, L.C.;
 Rodríguez-Parra, L.A.; Ramírez, V.; Niño, H. 2015.
 Middle Miocene closure of the Central American seaway. Science 348 (6231): 226-229.
- Montes, C.; Rodríguez-Corcho, A.F.; Bayona, G.; Hoyos, N.; Zapata, S.; Cardona, A. 2019. Continental margin response to multiple arc-continent collisions: The northern Andes-Caribbean margin. Earth-Science Reviews 198: 102903.
- Morimoto, N. 1989. Nomenclature of pyroxenes. Mineralogical Journal 14 (5): 198-221.
- Murcia, H.; Németh, K. 2020. EffusiveMonogenetic Volcanism. Volcanoes-Updates in Volcanology.

- IntechOpen. doi: https://doi.org/10.5772/intechopen. 94387
- Nakamura, N. 1974. Determination of REE,Ba,Fe,Mg,Na and K in carbonaceous and ordinary chondrites. Geochimica et Cosmochimica Acta 38 (5): 757-775.
- Nelson, S.T.; Montana, A. 1992. Sieve-textured plagioclase in volcanic rocks produced by rapid decompression. American Mineralogist 77 (11-12): 1241-1249.
- Pardo-Casas, F.; Molnar, P. 1987. Relative motion of the Nazca (Farallon) and South American plates since Late Cretaceous time. Tectonics 6 (3): 233-248.
- Pearce, T.H.; Kolisnik, A.M. 1990. Observations of plagioclase zoning using interference imaging. Earth-Science Reviews 29 (1-4): 9-26.
- Piedrahita, V.A.; Bernet, M.; Chadima, M.; Sierra, G.M.; Marín-Cerón, M.I.; Toro, G.E. 2017. Detrital zircon fission-track thermochronology and magnetic fabric of the Amagá Formation (Colombia): Intracontinental deformation and exhumation events in the northwestern Andes. Sedimentary Geology 356: 26-42.
- Piedrahita, D.A.; Murcia, H.; Arnosio, M. 2019. Características sedimentológicas y composicionales de la Formación Combia: propuesta de un modelo evolutivo del sistema magmático. *In* Congreso Colombiano de Geología No. 17. Santa Marta.
- Putirka, K.D. 2008. Thermometers and barometers for volcanic systems. Reviews in Mineralogy and Geochemistry 69 (1): 61-120.
- Ramírez, D.A.; López, A.; Sierra, G.M.; Toro, G.E. 2006. Edad y proveniencia de las rocas volcánico sedimentarias de la Formación Combia en el suroccidente Antioqueño-Colombia. Boletín de Ciencias de la Tierra 19: 9-26.
- Restrepo, J.J.; Toussaint, J.F.; González, H. 1981.
 Edades Mio-pliocenas del magmatismo asociado a la Formación Combia, departamentos de Antioquia y Caldas, Colombia. Geología Norandina 3: 21-26.
- Rodríguez, G.; Zapata, G. 2012. Características del plutonismo Mioceno superior en el segmento norte de la Cordillera Occidental e implicaciones tectónicas en el modelo geológico del noroccidente colombiano. Boletín de Ciencias de la Tierra (31): 5-22.
- Santacruz, L.; Redwood, S.D.; Cecchi, A.; Matteini, M.; Botelho, N.F.; Ceballos, J.; Starling, T.; Molano, J.C. 2021. The age and petrogenesis of reduced to weakly oxidized porphyry intrusions at the Marmato gold deposit, Colombia. Ore Geology Reviews 131: 103953.
- Seaman, S.J. 2000. Crystal clusters, feldspar glomerocrysts, and magma envelopes in the Atascosa Lookout lava flow, southern Arizona, USA: recorders of magmatic events. Journal of Petrology 41 (5): 693-716.

- Shcherbakov, V.D.; Plechov, P.Y.; Izbekov, P.E.; Shipman, J.S. 2011. Plagioclase zoning as an indicator of magma processes at Bezymianny Volcano, Kamchatka. Contributions to Mineralogy and Petrology 162 (1): 83-99.
- Sierra, G.M.; Marín-Cerón, M.I. 2011. Amagá, Cauca and Patía Basins. Petroleum Geology of Colombia, ANH-EAFIT 2: 104 p.
- Sierra, G.M.; Sierra, M.I.; Ríos, A.M. 2005. Registro del volcanismo Neógeno y la sedimentación fluvial en el suroeste antioqueño. Boletín de Ciencias de la Tierra 17: 135-152.
- Siivola, J.; Schmid, R. 2007. List of mineral abbreviations. En: Metamorphic Rocks: A Classification and Glossary of Terms. Recommendations of the International Union of Geological Sciences Subcommission on the Systematics of Metamorphic Rocks 22 (5): 93-110.
- Silva-Tamayo, J.C.; Sierra, G.M.; Correa, L.G. 2008. Tectonic and climate driven fluctuations in the stratigraphic base level of a Cenozoic continental coal basin, northwestern Andes. Journal of South American Earth Sciences 26 (4): 369-382.
- Somoza, R.; Ghidella, M.E. 2005. Convergencia en el margen occidental de América del Sur durante el Cenozoico: subducción de las placas de Nazca, Farallón y Aluk. Revista de la Asociación Geológica Argentina 60 (4): 797-809.
- Sosa-Ceballos, G.; Boijseauneau-López, M.E.; Pérez-Orozco, J.D.; Cifuentes-Nava, G.; Bolos, X.; Perton, M.; Simon-Velázquez, D. 2021. Silicic magmas in the Michoacan-Guanajuato volcanic field: An overview of plumbing systems, crustal storage, and genetic processes. Revista Mexicana de Ciencias Geológicas 38 (3): 210-225.
- Spikings, R.; Cochrane, R.; Villagómez, D.; Van der Lelij, R.; Vallejo, C.; Winkler, W.; Beate, B. 2015. The geological history of northwestern South America: from Pangaea to the early collision of the Caribbean Large Igneous Province (290-75 Ma). Gondwana Research 27 (1): 95-139.
- Sun, S.S.; McDonough, W.F. 1989. Chemical and isotopic systematics of oceanic basalts: implications for mantle composition and processes. Geological Society, London, Special Publications 42 (1): 313-345.
- Tassinari, C.C.G.; Pinzon, F.D.; Ventura, J.B. 2008. Age and sources of gold mineralization in the Marmato

- mining district, NW Colombia: a Miocene-Pliocene epizonal gold deposit. Ore Geology Reviews 33 (3-4): 505-518.
- Tejada, M.; Betancourt, J.; Nivia, A.; Weber, M.; Gómez, J. 2007. Cartografía geológica y caracterización geoquímica de la Formación Combia en los alrededores de Jericó y Pueblorrico, Departamento de Antioquia-Colombia. *In* Congreso Colombiano de Geología. No. 11: 23 p. Bucaramanga.
- Tepley, I.F.J.; Davidson, J.P.; Clynne, M.A. 1999. Magmatic interactions as recorded in plagioclase phenocrysts of Chaos Crags, Lassen Volcanic Center, California. Journal of Petrology 40 (5): 787-806.
- Tsuchiyama, A. 1985. Dissolution kinetics of plagioclase in the melt of the system diopside-albite-anorthite, and origin of dusty plagioclase in andesites. Contributions to Mineralogy and Petrology 89 (1): 1-16.
- Ustunisik, G.; Kilinc, A.; Nielsen, R.L. 2014. New insights into the processes controlling compositional zoning in plagioclase. Lithos 200: 80-93.
- Vance, J. A. 1969. On synneusis. Contributions to Mineralogy and Petrology 24 (1): 7-29.
- Villagómez, D.; Spikings, R. 2013. Thermochronology and tectonics of the Central and Western Cordilleras of Colombia: Early Cretaceous-Tertiary evolution of the northern Andes. Lithos 160: 228-249.
- Wagner, L.S.; Jaramillo, J.S.; Ramírez-Hoyos, L.F.; Monsalve, G.; Cardona, A.; Becker, T.W. 2017. Transient slab flattening beneath Colombia. Geophysical Research Letters 44 (13): 6616-6623.
- Weber, M.; Duque, J.F.; Hoyos, S.; Cárdenas-Rozo, A.L.; Tapias, J.G.; Wilson, R. 2020. The Combia Volcanic Province: Miocene Post-Collisional Magmatism in the Northern Andes. The Geology of Colombia 3: 355-394.
- Zapata, S.; Patiño, A.; Cardona, A.; Parra, M.; Valencia, V.; Reiners, P.; Oboh-Ikuenobe, F.; Genezini, F. 2020. Bedrock and detrital zircon thermochronology to unravel exhumation histories of accreted tectonic blocks: An example from the Western Colombian Andes. Journal of South American Earth Sciences 103: 102715.
- Zimmer, M.M.; Plank, T.; Hauri, E.H.; Yogodzinski, G.M.; Stelling, P.; Larsen, J.; Singer, B.; Jicha, B.; Mandeville, C.; Nye, C.J. 2010. The role of water in generating the calc-alkaline trend: new volatile data for Aleutian magmas and a new tholeiitic index. Journal of Petrology 51 (12): 2411-2444.